DOI:10.1021/ic900035a

Inorganic Chemistry
Article

Synthesis, Structure and Charge Transport Properties of $Yb_5Al_2Sb_6$: A Zintl Phase with Incomplete Electron Transfer

Iliya Todorov,[†] Duck Young Chung,[†] Linhui Ye,[‡,§] Arthur J. Freeman,[†,§] and Mercouri G. Kanatzidis*[,†,∥]

[†]*Materials Science Division, Argonne National Laboratory, Argonne, Illinois 60439,* [‡]*College of Chemistry and Molecular Engineering, Peking University, Peking 100871, China,* [§]*Department of Physics and Astronomy, Northwestern University, Evanston, Illinois 60208, and* [∥]*Department of Chemistry, Northwestern University, Evanston, Illinois 60208*

Received January 8, 2009

We report the synthesis, structure, spectroscopic properties, charge and thermal transport, and electronic structure of a new member of the Zintl family, $Yb_5Al_2Sb_6$. The compound crystallizes in the $Ba_5Al_2Bi_6$ structure type and requires the addition of Ge or Si in the synthesis, which appears to act as a catalyst. $Yb_5Al_2Sb_6$ has an anisotropic structure with infinite anionic double chains cross-linked by Yb^{2+} ions. Polycrystalline ingots of $Yb_5Al_2Sb_6$ prepared in the presence of 0.5 mol equiv of Ge showed room-temperature conductivity, thermopower, and thermal conductivity of ∼1100 S/cm, ∼20 μV/K, and ∼3.8 W/m·K, respectively. Investigations of other solid solutions of $Yb_5Al_2Sb_6$, doping effects, and chemical modifications are discussed. Sr only partially replaces Yb in the structure leading to $Sr_{0.85}Yb_{4.15}Al_2Sb_6$. Electronic structure calculations performed using a highly precise full-potential linearized augmented plane wave method within the density functional theory scheme show the presence of a negative band gap and suggest incomplete electron transfer and a metallic character to the compound.

Introduction

Zintl compounds are made of very electropositive alkali, alkaline-, or rare-earth metals and electronegative p-block metals.[1−7] Because of the large difference in electronegativity of their constituents, these compounds are often viewed as salts resulting from complete electron transfer from the more to the less electronegative element. The degree of complexity in these compounds strongly depends on the level of reduction of the post-transition element.[8−13] Thus, the structures span from three-dimensional networks to lower-level formations such as layers, chains, clusters, and single-atom anions as the degree of reduction rises. In recent years, there has been considerable focus on polar intermetallic compounds, for example, Zintl phases, to identify new thermoelectric materials candidates.[14−19] Specifically, from a thermoelectric point of view, Zintl compounds can possess attractive properties such as thermal stability at very high temperatures, a fairly small band gap, and complex anionic frameworks stabilized by weakly bonded electropositive cations, which result in low lattice thermal conductivity.[20−24] A major drawback of this

*To whom correspondence should be addressed. E-mail: m-kanatzidis@northwestern.edu.

(1) Lei, X. W.; Zhong, G. H.; Li, M. J.; Mao, J. G. *J. Solid State Chem.* **2008**, *181*, 2448–2455.
(2) Mathieu, J.; Achey, R.; Park, J. H.; Purcell, K. M.; Tozer, S. W.; Latturner, S. E. *Chem. Mater.* **2008**, *20*, 5675–5681.
(3) Ugrinov, A.; Sen, A.; Reber, A. C.; Qian, M.; Khanna, S. N. *J. Am. Chem. Soc.* **2008**, *130*, 782–783.
(4) Via, S. Q.; Hullmann, J.; Bobev, S. *J. Solid State Chem.* **2008**, *181*, 1909–1914.
(5) Wendorff, M.; Rohr, C. *Z. Naturforsch., B: Chem. Sci.* **2007**, *62*, 1059–1070.
(6) Xia, S. Q.; Bobev, S. *J. Am. Chem. Soc.* **2007**, *129*, 10011–10018.
(7) Xia, S. Q.; Bobev, S. *J. Am. Chem. Soc.* **2007**, *129*, 4049–4057.
(8) Ganguli, A. K.; Gupta, S.; Corbett, J. D. *Inorg. Chem.* **2006**, *45*, 196–200.
(9) Leon-Escamilla, E. A.; Corbett, J. D. *Chem. Mater.* **2006**, *18*, 4782–4792.
(10) Kim, H.; Condron, C. L.; Holm, A. P.; Kauzlarich, S. M. *J. Am. Chem. Soc.* **2000**, *122*, 10720–10721.
(11) Rehr, A.; Kuromoto, T. Y.; Kauzlarich, S. M.; Delcastillo, J.; Webb, D. J. *Chem. Mater.* **1994**, *6*, 93–99.
(12) Margadonna, S.; Prassides, K.; Chondroudi, M.; Salvador, J. R.; Kanatzidis, M. G. *Chem. Commun.* **2005**, 5754–5756.
(13) Margadonna, S.; Prassides, K.; Fitch, A. N.; Salvador, J. R.; Kanatzidis, M. G. *J. Am. Chem. Soc.* **2004**, *126*, 4498–4499.
(14) Corbett, J. D. *Angew. Chem., Int. Ed.* **2000**, *39*, 670–690.
(15) Kauzlarich, S. M.; Brown, S. R.; Snyder, G. J. *Dalton Trans.* **2007**, *21*, 2099–2107.
(16) Kim, J. H.; Okamoto, N. L.; Kishida, K.; Tanaka, K.; Inui, H. *J. Appl. Phys.* **2007**, *102*, 034510.
(17) Snyder, G. J.; Toberer, E. S. *Nat. Mater.* **2008**, *7*, 105–114.
(18) Wang, X. J.; Tang, M. B.; Zhao, J. T.; Chen, H. H.; Yang, X. X. *Appl. Phys. Lett.* **2007**, *90*, 232107–3.
(19) Zaikina, J. V.; Schnelle, W.; Kovnir, K. A.; Olenev, A. V.; Grin, Y.; Shevelkov, A. V. *Solid State Sci.* **2007**, *9*, 664–671.
(20) Snyder, J.; Christensen, M.; Nishibori, E.; Calliat, T.; Iversen, B. B. *Nat. Mater.* **2004**, *3*, 458–463.
(21) Condron, C. L.; Kauzlarich, S. M.; Gascoin, F.; Snyder, G. J. *J. Solid State Chem.* **2006**, *179*, 2252–2257.
(22) Nolas, G. S.; Poon, J.; Kanatzidis, M. *MRS Bull.* **2006**, *31*, 199–205.
(23) Patschke, R.; Zhang, X.; Singh, D.; Schindler, J.; Kannewurf, C. R.; Lowhorn, N.; Tritt, T.; Nolas, G. S.; Kanatzidis, M. G. *Chem. Mater.* **2001**, *13*, 613–621.
(24) Schujman, S. B.; Nolas, G. S.; Young, R. A.; Lind, C.; Wilkinson, A. P.; Slack, G. A.; Patschke, R.; Kanatzidis, M. G.; Ulutagay, M.; Hwu, S. J. *J. Appl. Phys.* **2000**, *87*, 1529–1533.

Published on Web 4/17/2009

class of compounds is that most of them are air- and moisture-sensitive, primarily because of the highly electropositive elements such as alkali or alkaline-earth metals, which are easily attacked by moisture and expose the reduced Zintl framework to oxidation. However, substitution of the electropositive elements in a particular system of interest with proper rare-earth metals can result in substantially more covalent bonds with the Zintl framework that drastically improve the stability of the compounds.[25] Recently, in attempts to find new thermoelectric materials, several air-stable Zintl phases including Ba_6Ge_{24},[26] $Ba_4In_8Sb_{16}$,[27] $Yb_{11}GaSb_9$,[28] $Ba_8Al_{14}Si_{31}$,[29] Mg_3Sb_2,[21] and $BaGa_2Sb_2$[30] were reported. Moreover, the most promising example from this class of compounds, $Yb_{14}MnSb_{11}$,[31] has demonstrated a thermoelectric figure of merit ZT of ~1.0 at 1223 K. This finding confirms earlier suggestions that the Zintl class of compounds could be a good source of thermoelectric materials.[27] Here, we describe $Yb_5Al_2Sb_6$, a member of the Zintl family. The compound crystallizes in the $Ba_5Al_2Bi_6$ structure type and is isostructural and isoelectronic to $Yb_5In_2Sb_6$.[30] The circumstances of the synthetic chemistry of $Yb_5Al_2Sb_6$ are very unusual and intriguing because they require the addition of Ge in the reactions, even though this element is not incorporated into the structure. Investigations of phase formation, chemical modifications, doping effects, and preliminary charge and thermal transport properties on this compound are reported. In addition, electronic structure calculations done on $Yb_5Al_2Sb_6$ show that the compound is in fact metallic, owing to incomplete electron transfer from Yb atoms to Sb atoms.

Experimental Section

Synthesis. Initially, $Yb_5Al_2Sb_6$ was found as a minor phase from reaction with a nominal composition of YbAlSbGe. After the stoichiometry of the compound was elucidated from its structure determination, we attempted to synthesize $Yb_5Al_2Sb_6$ as a single phase. In order to obtain the compound in high yields according to the following procedures, small amounts of Ge are required in the reaction (see the Results and Discussion). The compound was synthesized in high yields by two methods: direct combination in a Nb ampule and arc melting under argon.

In a typical direct combination reaction, the elements, Yb (3.32 mmol), Al (1.33 mmol), Sb (4.00 mmol), and Ge (0.333 mmol), were mixed in a niobium ampule that is sealed by arc-welding under argon. Yb (Treibacher Industrie, pieces, 99.9%), and Al (Alfa Aesar, powder, 99.97%) were used as received, while Sb (Cerac, ingot, 99.999%) and Ge (Plasma Materials, pieces, 99.999%) were ground into powder. The niobium ampule was then placed in a fused-silica tube and flame-sealed under a vacuum. The assembly was heated at 950 °C for 2 days and cooled to room temperature at a rate of 1 °C/min. The obtained product was in the form of loose crystals.

Arc melting under an argon atmosphere is another method used to produce this phase in the form of an ingot by using YbSb (2.5 mmol), Sb (0.5 mmol), Al (1 mmol), and Ge (0.5 mmol). YbSb prepared by direct combination in a niobium ampule was used, instead of pure elements, in order to minimize the Yb evaporation at high temperatures. The sample preparation for property measurements was performed by this method because it gives large ingots that can be easily cut and polished.

Elemental Analysis. The semiquantitative microprobe analysis of the compound was performed with a Hitachi S-2700 Scanning Electron Microscope using a Noran System Six Energy Dispersive Spectroscope (EDS) equipped with a thin window detector. Data were acquired by applying 20 kV of accelerating voltage. The results reported are an average of multiple quantifications on several single crystals. The EDS analysis on visibly clean surfaces of $Yb_5Al_2Sb_6$ crystals gave an atomic composition of 34.27% Yb, 40.62% Sb, and 25.12% Al. No Ge was found by EDS in any of the crystals we examined. The high error in Al concentration is caused by the Al-base stub used as a sample holder.

Charge Transport Measurements. For Seebeck coefficient and electrical conductivity measurements, arc-melted samples were cut into a rectangular shape and measured on the ULVAC ZEM-3 instrument. The thermal diffusivity and heat capacity of $Yb_5Al_2Sb_6$ were measured by laser flash techniques with a Netzsch LFA 457 system in a He atmosphere using a pyroceram standard for heat capacity measurements. The thermal conductivity was calculated from the experimental density, the heat capacity, and measured thermal diffusivity.

Differential Thermal Analysis. Differential thermal analysis (DTA) measurements were carried out with a Shimadzu DTA-50 thermal analyzer. The ground sample (80.0 mg total mass) was sealed in a quartz ampule under a vacuum. A silica ampule containing alumina of equal mass was sealed and placed as a reference. The sample was heated to 1100 at 10 °C/min, followed by cooling at the same rate to 50 °C. The stability and reproducibility of the sample was monitored by running multiple heating and cooling cycles.

Electronic Band Structure Calculations. The electronic structure calculations were performed using the full-potential linearized augmented plane wave (FLAPW) method[32] within the density functional scheme. The experimental lattice parameters and atomic coordinates were employed for the calculations. The core states and the valence states were treated fully relativistically and scalar relativistically, respectively. The spin−orbit interaction was also included self-consistently by a second variational method.[33] The muffin-tin radii of Yb, Al, and Sb are chosen to be 3.1, 2.3, and 2.7, respectively. The plane-wave cutoff is $|\mathbf{k} + \mathbf{G}| \leq 3.5$, and the star-function cutoff is 8.1. All units are in atomic units. The Brillouin zone integration is replaced by the special **k**-point summation on the $1 \times 5 \times 3$ Monkhorst−Pack mesh, corresponding to the experimental lattice constants of $a_1 = 23.118$ Å, $a_2 = 4.4497$ Å, and $a_3 = 7.3313$ Å. Experimentally, the $Yb_5Al_2Sb_6$ compound shows poor metallic conductivity. The possibility of $Yb_5Al_2Sb_6$ being a small gap semiconductor was checked by comparing the calculations using both LDA and screened exchange LDA (sx-LDA) separately as the exchange-correlation potential. The spin−orbit coupling effect is also included in our sx-LDA calculations by the second variational method.[33] Convergence of our results has been tested by repeating the LDA calculations

(25) Chan, J. Y.; Olmstead, M. M.; Kauzlarich, S. M.; Webb, D. J. *Chem. Mater.* **1998**, *10*, 3583–3588.
(26) Kim, S.-J.; Hu, S.; Uher, C.; Hogan, T.; Huang, B.; Corbett, J. D.; Kanatzidis, M. G. *J. Solid State Chem.* **2000**, *153*, 321–359.
(27) Kim, S.-J.; Hu, S.; Uher, C.; Kanatzidis, M. G. *Chem. Mater.* **1999**, *11*, 3154–3159.
(28) Bobev, S.; Fritschb, V.; Thompson, J. D.; Sarraob, J. L.; Eckc, B.; Dronskowski, R.; Kauzlarich, S. M. *J. Solid State Chem.* **2005**, *178*, 1071–1079.
(29) Condron, C. L.; Martin, J.; Nolas, G. S.; Piccoli, P. M. B.; Schultz, A. J.; Kauzlarich, S. M. *Inorg. Chem.* **2006**, *45*, 9381–9386.
(30) Kim, S.-J.; Ireland, J. R.; Kannewurf, C. R.; Kanatzidis, M. G. *J. Solid State Chem.* **2000**, *155*, 55–61.
(31) Brown, S. R.; Kauzlarich, S. M.; Gascoin, F.; Snyder, G. J. *Chem. Mater.* **2006**, *18*, 1873–1877.
(32) Wimmer, E.; Krakauer, H.; Weinert, M.; Freeman, A. *J. Phys. Rev. B* **1981**, *24*, 864–875.
(33) MacDonald, A. H.; Pickett, W. E.; Koelling, D. D. *J. Phys. C: Solid State Phys.* **1980**, *13*, 2675–2683.

Table 1. Selected Data Collection and Refinement Parameters for $Yb_5Al_2Sb_6$ and $Sr_{0.85}Yb_{4.15}Al_2Sb_6$

empirical formula	$Yb_5Al_2Sb_6$	$Sr_{0.85}Yb_{4.15}Al_2Sb_6$
fw	1649.66	1572.78
temp	293(2) K	293(2) K
wavelength	0.71073 Å	0.71073 Å
cryst syst	orthorhombic	orthorhombic
space group	*Pbam*	*Pbam*
unit cell dimensions	a = 7.2971(15) Å	a = 7.3313(15) Å
	b = 22.780(5) Å	b = 23.118(5) Å
	c = 4.4115(9) Å	c = 4.4497(9) Å
vol	733.3(3) Å^3	754.2(3) Å^3
Z	2	2
density (calcd)	7.471 Mg/m^3	6.926 Mg/m^3
abs coeff (calcd)	42.459 mm^{-1}	38.922 mm^{-1}
F(000)	1364	1306
cryst size	0.3 × 0.03 × 0.018 mm	0.3 × 0.09 × 0.05 mm
reflns collected/unique	8105/1401	9843/1617
data/restraints/params	1401/0/42	1617/0/43
goodness-of-fit on F^2	1.139	1.094
final R indices $[F_0^2 > 2\sigma(F_0^2)]$[a]	R_1/wR_2 = 2.99/7.00%	R_1/wR_2 = 3.42/8.84%
R indices ($F_0^2 > 0$)	R_1/wR_2 = 3.31/7.10%	R_1/wR_2 = 3.69/8.99%

[a] $R_1 = [\sum||F_0| - |F_c||]/\sum|F_0|$. $wR_2 = \{[\sum w(|F_0| - |F_c|)_2/[\sum w(F_0^2)]]\}_{1/2}$. $w = \sigma_F^2$.

Table 2. Atomic Coordinates (× 10^4) and Equivalent Isotropic Displacement Parameters (Å^2 × 10^3) for $Yb_5Al_2Sb_6$

	x	y	z	U(eq)[a]
Yb(1)	5484(1)	888(1)	0	11(1)
Yb(2)	10000	0	0	12(1)
Yb(3)	7332(1)	2524(1)	0	9(1)
Sb(4)	9744(1)	1357(1)	0	9(1)
Sb(5)	4868(1)	1883(1)	5000	9(1)
Sb(6)	2994(1)	51(1)	5000	10(1)
Al(1)	1839(4)	1218(1)	5000	11(1)

[a] Note, U(eq) is defined as one-third of the trace of the orthogonalized U^{ij} tensor.

Table 3. Anisotropic Displacement Parameters (Å^2 × 10^3) for $Yb_5Al_2Sb_6$[a]

	U^{11}	U^{22}	U^{33}	U^{23}	U^{13}	U^{12}
Yb(1)	14(1)	8(1)	11(1)	0	0	1(1)
Yb(2)	10(1)	10(1)	16(1)	0	0	1(1)
Yb(3)	6(1)	8(1)	13(1)	0	0	0(1)
Sb(4)	7(1)	7(1)	13(1)	0	0	−1(1)
Sb(5)	8(1)	9(1)	8(1)	0	0	−1(1)
Sb(6)	9(1)	10(1)	10(1)	0	0	2(1)
Al(1)	10(1)	11(1)	13(1)	0	0	−2(1)

[a] Note, the anisotropic displacement factor exponent takes the form $-2^2[h^2a^{*2}U^{11} + ... + 2hka^*b^* U^{12}]$.

with increased plane-wave and star function cutoffs and doubled special **k**-point mesh. We found no obvious change in the final LDA band structure, which proved that our chosen computational parameters are indeed appropriate.

Structure Determination. For X-ray crystallographic studies, a black bar-shaped crystal was mounted on a glass fiber. For this crystal, with dimensions of 0.3 × 0.03 × 0.018 mm^3, a half-sphere of reciprocal space up to 63.68° in 2θ was collected on a STOE image plate diffractometer using graphite monocromatized Mo Kα radiation. The individual frames were measured with a ω rotation of 1° and exposure time of 1 min. No crystal decay was detected. The observed Laue symmetry and systematic extinctions were indicative of the space groups *Pbam* and *Pba*2. The centrosymmetric *Pbam* space group was assumed, and subsequent refinements confirmed the correct choice of this space group. The initial positions of all atoms were obtained by direct methods. The structure was refined by full-matrix least-squares techniques with the SHELXTL[34] package of crystallographic programs. Once all atoms were located, the occupancies of successive atoms were allowed to vary, but refinements did not lead to any significant change in the occupation factor. After anisotropic refinement of all atoms, a difference electron density Fourier map calculated with phases based on the final parameters showed maximum and minimum peaks of +3.034 and −3.192 e/Å^3, respectively. The complete data collection parameters, details of structure solution, and refinement results are given in Table 1. Final atomic positions, displacements parameters, and anisotropic displacement parameters are given in Tables 2 and 3. Selected bond distances and angles are listed in Table 4.

Table 4. Bond Lengths [Å] and Angles [deg] for $Yb_5Al_2Sb_6$

Sb1−Al1 × 2	2.7027(17)	Yb1−Al1 × 2	3.536(2)
Sb2−Al1	2.680(3)	Yb2−Sb1 × 2	3.0966(8)
Sb3−Al1	2.787(3)	Yb2−Sb3 × 4	3.1066(6)
Sb3−Sb3	2.9375(1)	Yb3−Sb1	3.1719(8)
Yb1−Sb2 × 2	3.1957(7)	Yb3−Sb2 × 2	3.1796(6)
Yb1−Sb3 × 2	3.2671(6)	Yb3−Sb1	3.1893(8)
Yb1−Sb1	3.2868(9)	Yb3−Sb2 × 2	3.1987(6)
Yb1−Sb3 × 2	3.4346(7)	Yb3−Al1 × 2	3.634(2)
Yb1−Yb2	3.8661(7)	Yb1−Yb1	4.1050(11)
Yb1−Yb3	3.9651(9)	Yb3−Yb3	3.6503(8)
Al1−Sb1−Al1	109.40(10)	Sb1−Al1−Sb1	109.40(10)
Al1−Sb3−Sb3	112.16(6)	Sb2−Al1−Sb3	106.86(10)
Sb2−Al1−Sb1	113.60(7)	Sb1−Al1−Sb3	106.42(7)

Results and Discussion

Synthesis and Characterization. The most interesting aspect of the synthesis of $Yb_5Al_2Sb_6$ is the necessity of having Ge in the reaction. All products obtained from reactions without the addition of Ge showed $Yb_{11}Sb_{10}$ as a major phase, and the new phase $Yb_5Al_2Sb_6$ could not be detected even as a minor phase by powder X-ray diffraction (PXRD). Single crystals of $Yb_5Al_2Sb_6$ could only be obtained by adding Ge in the reaction. The phase was obtained in very high yield (95% based on Yb) if the molar equivalent of Ge per formula unit was between 0.25 and 0.5. Below 0.25 equiv of Ge, other phases such as YbSb and $Yb_{11}Sb_{10}$ were observed in the PXRD pattern. Crystals of $Yb_5Al_2Sb_6$ did not contain any Ge in their structure, as determined by microprobe elemental analyses and by the X-ray single-crystal structure refinement. Later, it was found that Si plays a similar role in the formation process of the new phase, but only when arc-melting was used for the preparation of the compound. Direct combination reactions with Si instead of Ge did not produce $Yb_5Al_2Sb_6$. Presumably, this difference is due to the higher melting point of Si compared to Ge and implies that these two elements have to be molten for the successful synthesis of $Yb_5Al_2Sb_6$.

The role of Ge and Si in the reaction to produce $Yb_5Al_2Sb_6$ phase in high yield is not fully understood. One could speculate that Ge and Si act as catalysts or that Al, Ge (or Si), and Sb form a low-temperature eutectic that probably prevents the formation of the more thermodynamically stable binary Yb/Sb phases. It should be noted that there are no reported experimental or theoretical

(34) In *SHELXTL*, 5th ed.; Siemens Analytical X-ray Systems, Inc.: Madison, WI, 1994.

ternary Al/Ge/Sb phase diagrams. The samples examined here are denoted as $Yb_5Al_2Sb_6/x$Ge, where x is the equivalent of Ge applied in the synthesis as a reaction agent.

Thermal and Spectroscopic Analysis. $Yb_5Al_2Sb_6$ appears stable in the air and at room temperature. Crystals exposed to ambient air for a week did not show signs of decomposition, as judged by X-ray diffraction. The compound however reacts with water and decomposes to $YbSb_2$, YbO, $Yb_2Al_5O_{12}$, and other amorphous phases which we could not identify. The DTA analysis of samples of $Yb_5Al_2Sb_6$ up to 1100 °C did not show any melting/crystallization peaks. An energy band gap was observed in the form of a broad absorption in the mid-IR region in the range of 0.3−0.4 eV, suggesting that the material is probably a narrow gap semiconductor. Electronic structure calculations, however, and charge transport measurements, to be presented below, show that the compound is in fact metallic. Therefore, the observed feature at 0.3 eV is likely from a higher-level excitation.

Crystal Structure. $Yb_5Al_2Sb_6$ crystallizes in the $Ba_5Al_2Bi_6$[35−38] structure type. The structure consists of $^1_\infty[(Al_2Sb_6)^{10-}]$ double chains. The double chains form from the condensation of interconnected $AlSb_4$ tetrahedra bridged by Sb−Sb bonds, Figures 1 and 2. Neighboring infinite double chains are crystallographically equivalent and related by *b*-glide and *a*-glide symmetry operations perpendicular to the *a* and *b* directions and are separated by Yb cations.

The tetrahedral units $PnSb_4$ (Pn = Al, Ga) are very stable, which results in a relatively large number of ternary compounds. For example, such tetrahedra have been found in $Yb_{11}GaSb_9$[28] and its isostructural analogs, while in the A_3MPn_3 family, they form oligomeric and polymeric entities. The use of cations with different sizes, Ba or Ca, results in the formation of two distinct units: (1) dimeric anion $[Al_2Sb_6]^{12-}$ formed from two tetrahedrons sharing a common edge found in Ba_3AlSb_3[35,36] and (2) polymeric chain $^1_\infty[AlSb_6^{3-}]$ made of two corner-sharing tetrahedra found in Ca_3AlSb_3.[36] $Yb_5Al_2Sb_6$ also can be viewed as a derivative of Ba_3AlSb_3 ($Ba_6Al_2Sb_6$). Upon virtual removal of one Ba cation, the anions $[Al_2Sb_6]^{12-}$ oxidatively couple via Sb−Sb bridges to form $^1_\infty[Al_2Sb_6^{10-}]$ infinite double chains found in the title compound. The Sb−Sb distance in $Yb_5Al_2Sb_5$ of 2.937(1) Å (Figure 2) is comparable to that in $Yb_5In_2Sb_6$ but is longer compared to the Sb−Sb distance (2.906 Å) in alkaline-earth isostructural compound $Ca_5Al_2Sb_6$.

The Yb atoms occupy three crystallographically unique positions in the structure. The Yb−Sb distances are in the range of 3.0966(8)−3.7346(7) Å, with the longest being observed for Yb(1)−Sb(3). Yb(2) and Yb(3) are in distorted octahedral coordination, while Yb(1) is seven-coordinated in a capped trigonal prismatic geometry (Figure 3). The coordination environment of the Yb atoms is similar to that of the Ca atoms in $Ca_5Al_2Sb_6$, which crystallizes in a different structure type, that is,

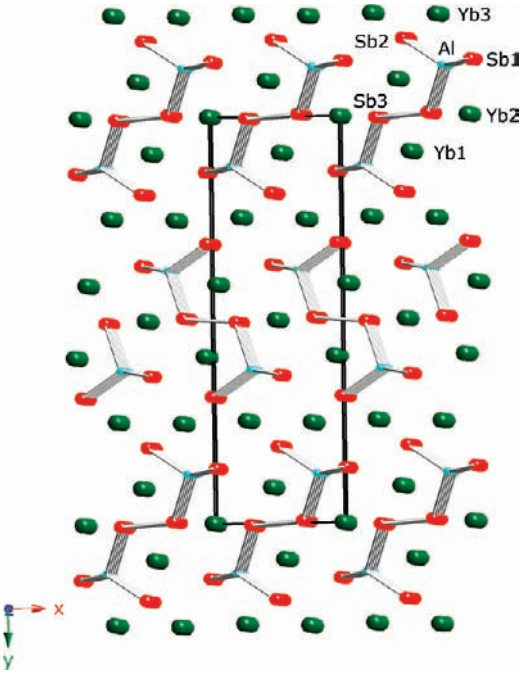

Figure 1. A projection of the structure of $Yb_5Al_2Sb_6$ along the *c* axis.

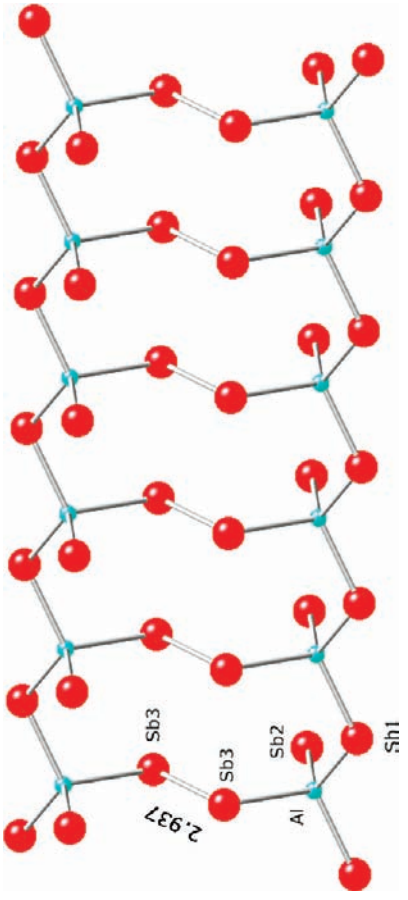

Figure 2. The ladder-type structure of one double chain of tetrahedra bridged by Sb−Sb bonds.

$Ca_5Ga_2As_6$. The major difference between these two structure types, $Ba_5Al_2Bi_6$ and $Ca_5Ga_2As_6$, lies in the coordination environment of Yb(3) and Ca(3) atoms in this case. Ca(3) is in ideal octahedral geometry and is surrounded by only two Sb(3) atoms. On the other hand,

(35) Cordier, G.; Savelsberg, G.; Schaefer, H. *Z. Naturforsch., B: Chem. Sci.* **1982**, *37*, 975–980.
(36) Cordier, G.; Schaefer, H.; Stelter, M. *Z. Naturforsch., B: Chem. Sci.* **1984**, *39*, 727–732.
(37) Cordier, G.; Schaefer, H.; Stelter, M. *Z. Naturforsch., B: Chem. Sci.* **1985**, *40*, 5–8.
(38) Cordier, G.; Schaefer, H.; Stelter, M. *Z. Naturforsch.* **1985**, B40.

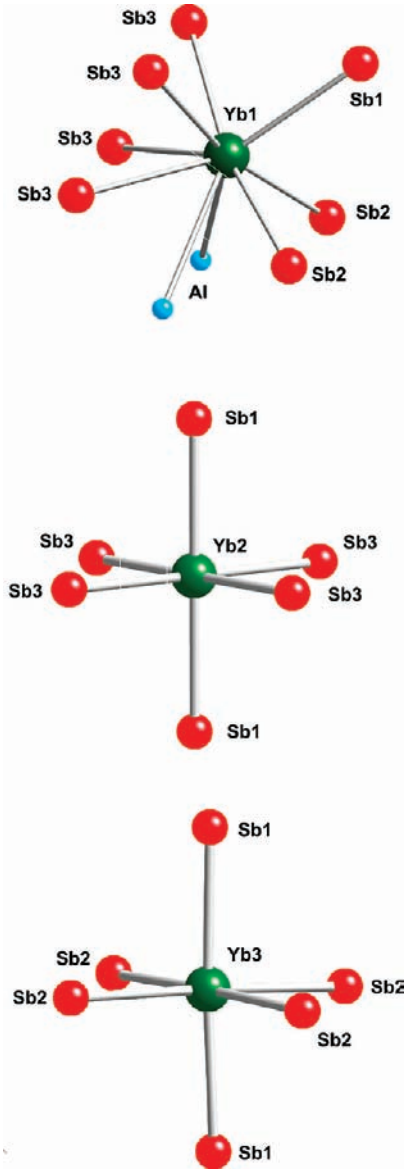

Figure 3. The immediate coordination environment (up to 3.6 Å) of the three Yb atoms.

Yb(3)'s position in the new compound is in a distorted octahedral geometry and surrounded by four Sb(3) atoms. Electronic structure calculations done on members from both structure types suggest that the structure difference arises from different orbital mixing interactions, between the cation and anionic frameworks.[39,40] Therefore, compounds crystallizing in the $Ba_5Al_2Bi_6$ structure type are more covalent and have narrower band gaps compared to those of $Ca_5Ga_2As_6$-type compounds.

$Yb_5Al_2Sb_6$ contains cationic and anionic substructures and is therefore a polar intermetallic. The formula can be easily rationalized according to the Zintl−Klemm concept. Assuming complete electron transfer, the resulting 10 electrons from Yb are distributed over the repeating unit, Al_2Sb_6. The formal charge of tetrahedral Al is −1, while one- and two-bonded Sb atoms carry a charge of −2 and −1, respectively. Thus, in the Zintl convention, the formula can be rewritten as $(Yb_5^{2+})[2(Al^-)\cdot 4(Sb^-)\cdot 2(Sb^{2-})]$. An alternative, more intuitive, and preferable electron counting scheme based on cations and anions is $(Yb^{2+})_5[(Al^{3+})_2(Sb_2^{4-})(Sb^{3-})_4]$.

Charge Transport and Thermal Transport Properties of $Yb_5Al_2Sb_6$. The electrical conductivity and thermopower of arc-melted ingots of $Yb_5Al_2Sb_6$ synthesized with different mixtures of Ge and Si were measured as a function of the temperature. These samples were annealed at 600 °C before the property measurements in order to release any physical stress created by arc-melting. Measurements performed before and after annealing showed significant effects on the electrical conductivity but not the thermopower. For samples of $Yb_5Al_2Sb_6$ prepared with 0.5Ge, the conductivity at room temperature was ∼1100 S/cm and decreased slowly with increasing temperature, Figure 4a. This can be attributed to the decrease in carrier mobility with rising temperature, as expected for metals or heavily doped semiconductors. This apparent metallic dependence is supported by the electronic structure calculations presented below. The corresponding value of thermoelectric power was ∼20 μV/K at room temperature and increased almost linearly with increasing temperature. The positive thermopower values indicate that the material $Yb_5Al_2Sb_6$ is a p-type (hole) conductor.

The room-temperature thermal conductivity of $Yb_5Al_2Sb_6$ was measured at 3.8 W/m·K. The thermal conductivity is composed of the electronic component, which depends only on the electrical conductivity σ, according to the Wiedemann−Franz law $L = k_{el}\sigma T$ (the Lorenz number $L = 2.45 \times 10^{-8}$ W Ω K^{-2}), and the lattice component strongly depends on lattice vibrations (phonons). The lattice contribution of $Yb_5Al_2Sb_6$/0.5Ge at ∼3 W/m K is approximately 80% of the total thermal conductivity at room temperature (Figure 4b). The thermal conductivity is relatively low for a metal but somewhat higher than those of good thermoelectric materials.[41]

The investigation of this phase with various combinations of different reaction agents added as potential dopants including Te and SiGe alloys as well as Ge and Si did not show significant changes in the thermopower (Figure 5a), but apparent changes in the electrical conductivity were observed (Figure 5b). The highest room-temperature value (2839 S/cm) was observed for $Yb_5Al_2Sb_6$ prepared with 0.5Ge0.5Te, while the lowest (623 S/cm) was observed for $Yb_5Al_2Sb_6$/0.5Si.

As a Zintl phase, $Yb_5Al_2Sb_6$ is susceptible to chemical modifications because of its saltlike nature. In general, the anionic part of the structure $^1_\infty[(Al_2Sb_6)^{10-}]$ is responsible for the carrier mobilities; therefore, structural changes in the anionic framework are expected to affect the conductivity and thermopower. On the other hand, the cationic part is very prone to doping and site disorder. This causes little to no change in the anionic part of the structure, thus keeping the conductivity and Seebeck coefficient relatively constant. Therefore, increased phonon scattering by mass fluctuation in the cation sites may lower the lattice thermal conductivity

(39) Lam, R.; Mar, A. *Inorg. Chem.* **1996**, *35*, 6959–6963.
(40) Lam, R.; Zhang, J.; Mar, A. *J. Solid State Chem.* **2000**, *150*, 371–376.
(41) Chan, J. Y.; Olmstead, M. M.; Kauzlarich, S. M.; Webb, D. *J. Chem. Mater.* 1998, 10.

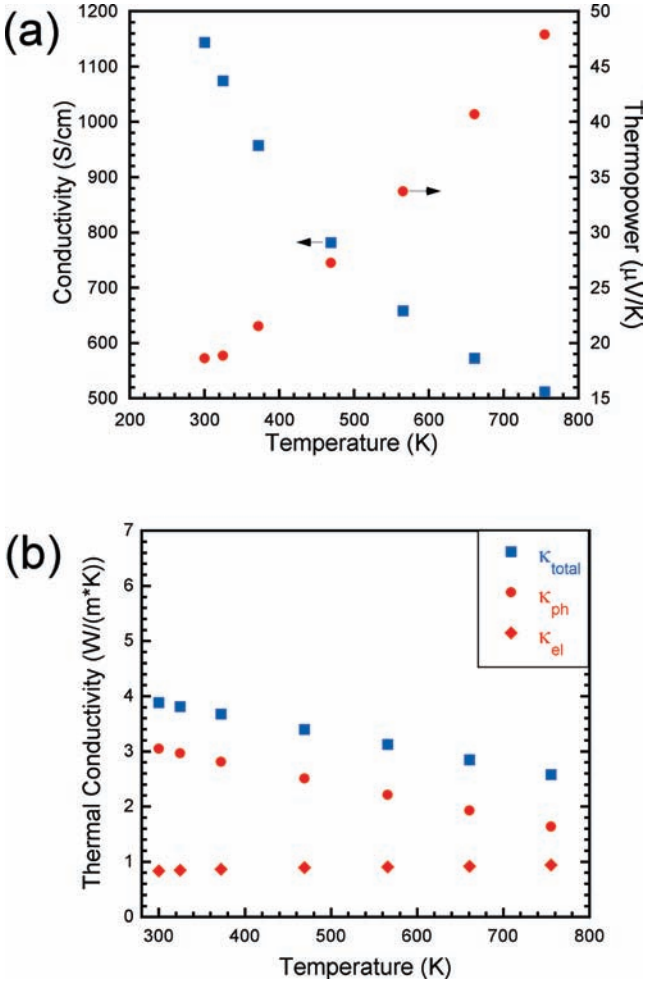

Figure 4. Variable-temperature (a) conductivity and thermopower and (b) total (κ_{total}), lattice (κ_{ph}), and electronic (κ_{el}) thermal conductivities for $Yb_5Al_2Sb_6$/0.5Ge.

and subsequently increase the figure of merit, ZT. A recent example representing the idea that the transport property of the Zintl phase can be finely tuned by substitution with a slightly more electropositive - cation is $Ca_xYb_{1-x}Zn_2Sb_2$.[42] The produced disorder by changing the Yb/Ca ratio indeed was reported to lower the lattice thermal conductivity, while the conducting anion substructure remains unchanged. This is evidenced by the relatively unchanged band gap and carrier mobility.

We have applied a similar approach here. In the case of $Yb_5Al_2Sb_6$, however, substitution with Ca was unsuccessful, and with Sr, only partially successful. Multiple syntheses designed for different Sr contents were attempted with 1:1 to 1:4 Yb/Sr ratios. Single crystals obtained from these different Sr/Yb ratios were analyzed with X-ray diffraction, Table 1 (tables of the atomic coordinates and anisotropic displacement parameters are provided as Supporting Information). Interestingly, the substitution was found successful only up to a Sr content of 17% and occurred preferably at the Yb(1) position. This is attributed to the fact that the atoms at this position are weakly coordinated and show the longest Sb···Yb contacts.

(42) Gascoin, F.; Ottensmann, S.; Stark, D.; Haile, S. M.; Snyder, J. *Adv. Funct. Mater.* **2005**, *15*, 1860–1864.

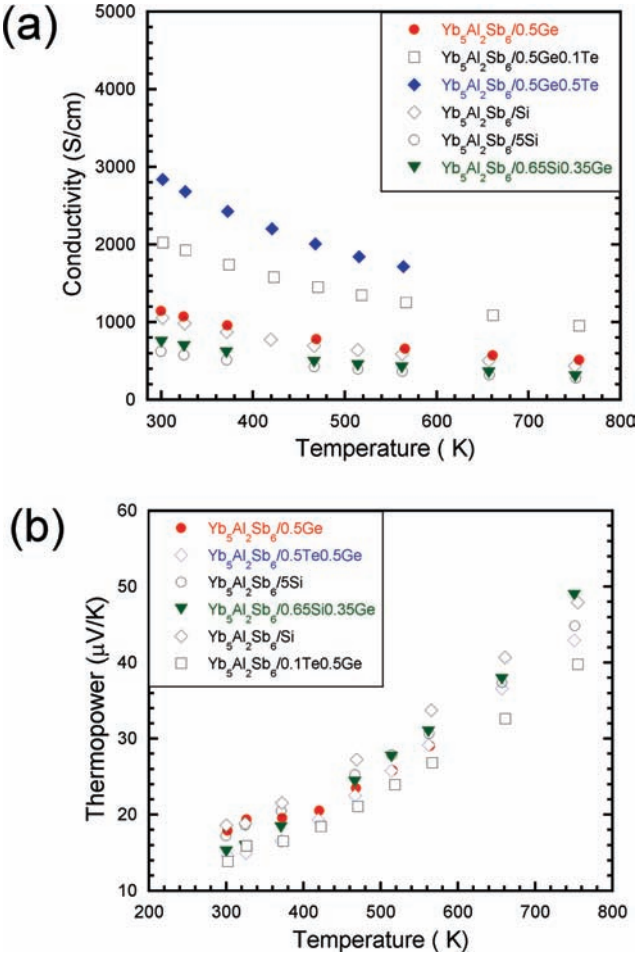

Figure 5. (a) Electrical conductivity and (b) thermopower for $Yb_5Al_2Sb_6$ prepared with different reaction agents (i.e., Ge and Si) and dopants.

The room-temperature total thermal conductivity drops significantly from ~3.8 W/m·K for $Yb_5Al_2Sb_6$ to ~2.5 W/m·K for $Sr_{0.85}Yb_{4.15}Al_2Sb_6$ prepared with 0.5Ge (Figure S1, see Supporting Information). The lattice component of the thermal conductivity of the Sr/Yb mixed compound is lower than that of parent Yb-only compound, presumably because of the increased phonon scattering induced by the Sr/Yb mass fluctuation in the cation sites. On the basis of the room-temperature electrical conductivity of $Sr_{0.85}Yb_{4.15}Al_2Sb_6$ of ~550 S/cm, we estimate a lattice thermal conductivity value of ~2 W/m·K.

Electronic Structure Calculations. The electronic structure of $Yb_5Al_2Sb_6$ was calculated by the highly precise FLAPW method. The LDA and sx-LDA band structures of $Yb_5Al_2Sb_6$ are shown in Figure 6 for comparison. It is clear that using the more sophisticated nonlocal exchange-correlation potential of sx-LDA does not bring about substantial changes in the band structure. The results suggest that the material is a metal or semimetal because the bottom of the conduction band reaches below the top of the valence band. The conduction and valence bands however do not cross, which means there is a negative band gap in the material, Figure 6b. This explains the metallic-like transport properties described above. The −9.5~12.0 eV bands derive predominantly from the Sb 5s. Al 3s bands appear

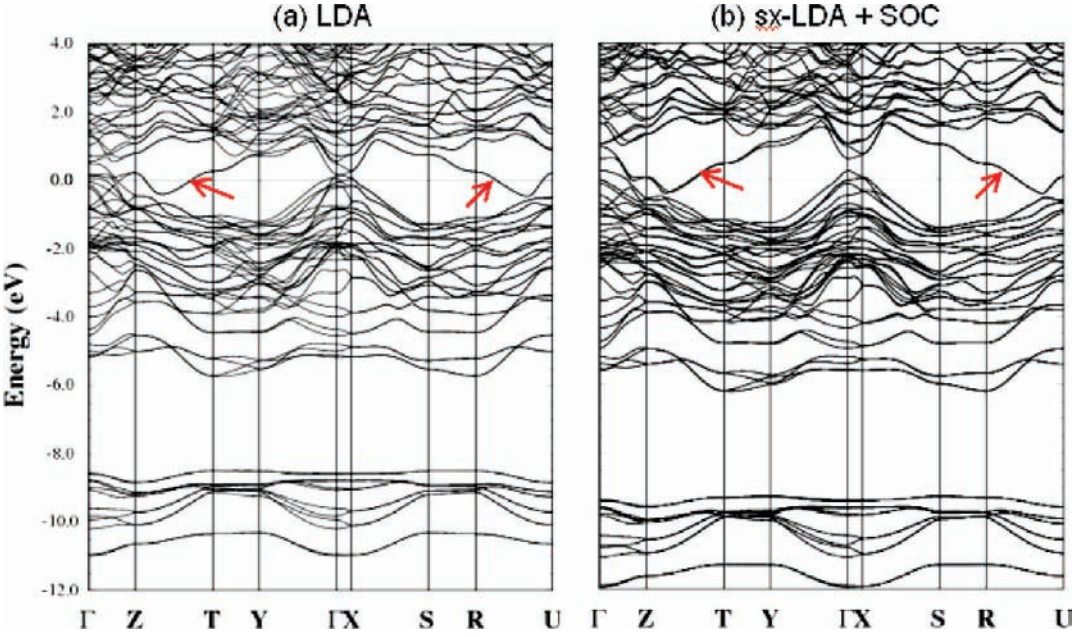

Figure 6. The LDA (left panel) and sx-LDA (right panel) band structures of $Yb_5Al_2Sb_6$. In the sx-LDA case, spin−orbit coupling is also included. The arrows are shown to indicate the so-called SYS bands described in the text.

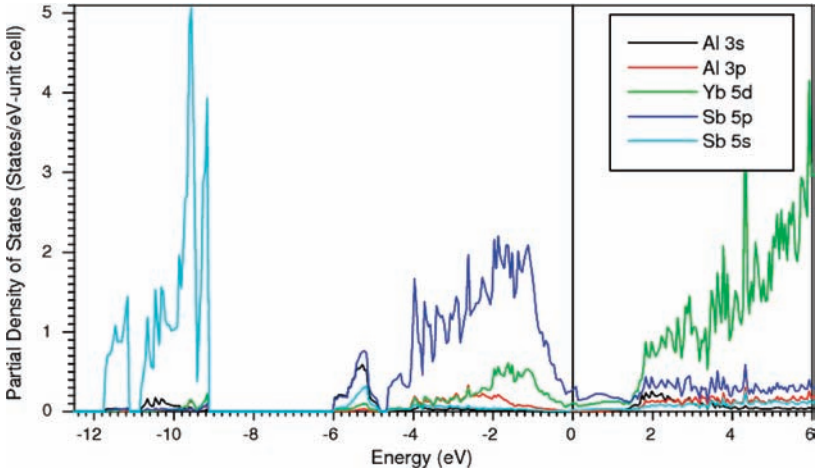

Figure 7. The projected density of states (pDOS) of $Yb_5Al_2Sb_6$ by sx-LDA including spin−orbit coupling.

at about −5.0 eV. Bands from −4.5 eV up to the E_F are mainly Sb 5p, which constitute most of the valence spectra. The conduction bands are mostly Yb 5d states. Moderate hybridization between Sb 5p and Yb 5d states is found in both the valence and the conduction bands close to E_F, as this is also clearly seen in the projected density of states in Figure 7.

One of the major effects of sx-LDA is that the valence bands are shifted downward in energy. This is due to the partial cancelation of the self-interaction error. Usually, the self-interaction correction is most significant for localized states. In the present case, the downward shift of the bands is not very obvious. This is because the valence window, which mainly consists of Sb 5s, Al 3s, and Sb 5p, does not contain strongly localized states. Another difference of the LDA and the sx-LDA band structures is found near Γ: by LDA, the conduction and valence bands are connected, while by sx-LDA, they are separated. Consequently, a pseudogap of 0.35 eV appears at Γ in the sx-LDA DOS close to E_F. Experimentally, a dip of about 0.3 eV close to E_F is found in the optical absorption spectra and could originate from this pseudogap in the DOS.

Between the high symmetry points Z and T, and R and U, four bands cross the E_F . We name them the SYS bands after their Sb−Yb−Sb characters, which we will illustrate in the following, see arrows in Figure 6. The four SYS bands are divided into two groups, each group being 2-fold degenerate. The splitting to the two groups is due to spin−orbit coupling, while the 2-fold degeneracy within each group comes from the equivalence of the two types of double chains, which have different orientations.

Compared to the majority of the valence bands, the SYS bands are obviously different concerning their unusual dispersions and their being much higher in energy. To understand why the SYS bands are well-separated from the majority of the valence bands, we plot in Figure 8 two wave functions: both wave functions are taken from the T point, with the first from the top of the valence

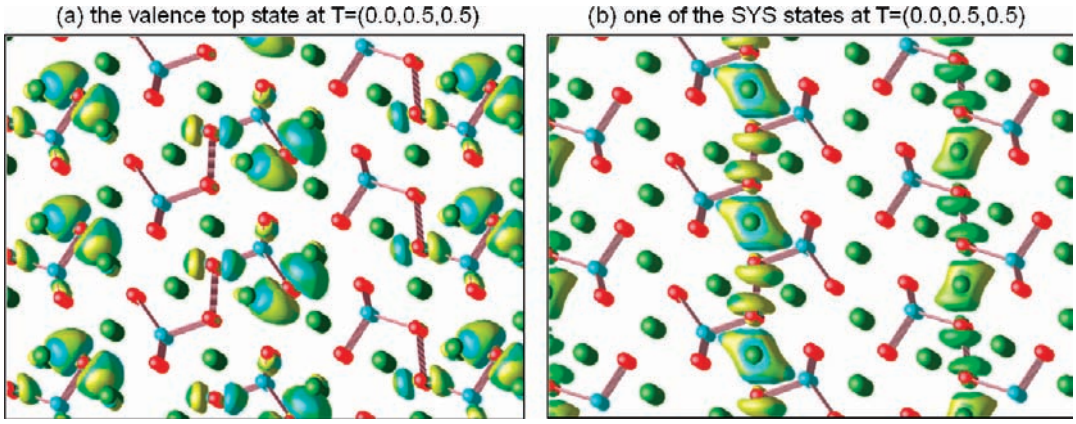

Figure 8. Plot of the two wave functions at $T = (0.0, 0.5, 0.5)$. Left panel: Wave function from the top of the valence band, which is intradouble-chain in character. Right panel: Wave function from one of the SYS bands, which is interdouble-chain in character. The Sb(*c*)−Yb−Sb(*c*) bonding provides a coupling between neighboring double chains.

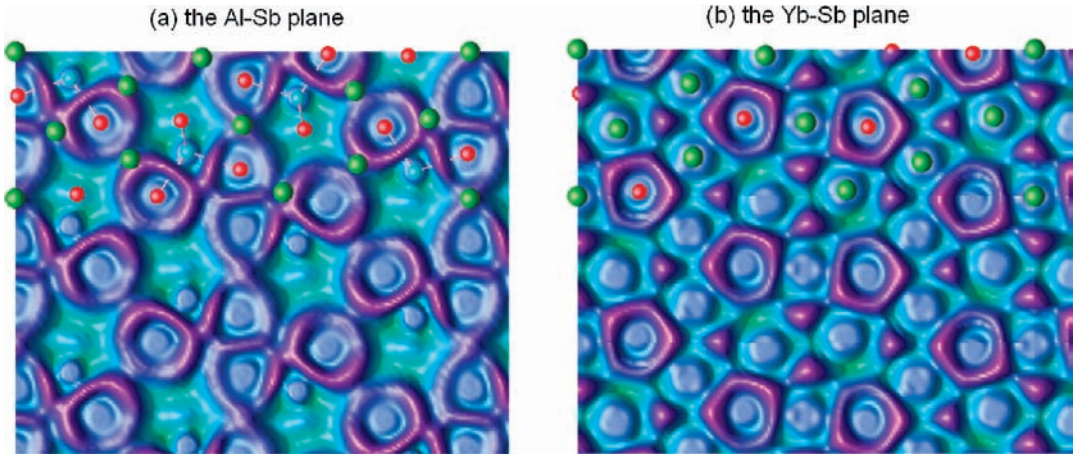

Figure 9. Charge redistribution in $Yb_5Al_2Sb_6$. Upper panel: Plot of the Al−Sb plane. Lower panel: Plot of the Yb−Sb plane. Charge transfer from the Al/Yb atoms to the Sb atoms in the $Yb_5Al_2Sb_6$ compound. Both the altitude and the color show the change of the electron density between the superposition of individual atomic densities and the total density of $Yb_5Al_2Sb_6$. Purple color shows electron accumulation, and green color shows electron depletion. (a) Plot on the Al−Sb plane, which illustrates the charge transfer from Al to Sb, and (b) plot on the Yb−Sb plane, which illustrates the charge transfer from Yb to Sb.

bands and the second from one of the SYS bands. It is clear that the first wave function (i.e., the one from the top of the valence bands) comes from the Sb(2) atoms. This wave function is mainly restricted within the one double chain and extends along the orientation of the chain. Therefore, this state is essentially one-dimensional. On the other hand, the second wave function (i.e., the one from the SYS bands) mainly comes from the Sb(3) atoms. These Sb(3) atoms are connected, not only within each double chain but also between neighboring double chains through the Sb(3)−Yb−Sb(3) bonding. This inter-double-chain character of the SYS bands explains why they are separated from the majority of the valence bands, which are mainly intra-double-chain in character.

It is hard to judge the chemical valence of each atom in $Yb_5Al_2Sb_6$, as the Al $n = 3$ shell is not completely empty and the Sb 5p subshell not completely full. To study the charge redistribution in $Yb_5Al_2Sb_6$, we plot the charge density difference between the $Yb_5Al_2Sb_6$ compound and the superposition of the individual atoms. In Figure 9, the plots of the Al−Sb plane and the Yb−Sb plane clearly show that charge accumulates at the Sb $n = 5$ shell, and that they are depleted from the regions close to the Al and the Yb atoms. This is consistent with the Zintl-type nature of the compound.

Concluding Remarks

The new compound, $Yb_5Al_2Sb_6$, forms from high-temperature reactions only when elemental Ge or Si is also present. In the absence of these elements, a different set of products forms. To our knowledge, this is the first example of a Zintl compound being stabilized in synthesis by another element (called here a reaction agent) even though this element is not incorporated in the structure. Although fluxes are known to stabilize metastable or kinetically stable compounds, they are usually present in excess.[43−45] Besides, in the case of $Yb_5Al_2Sb_6$, we have no indication that it is a metastable compound. The charge transport properties of

(43) Chondroudis, K.; McCarthy, T. J.; Kanatzidis, M. G. *Inorg. Chem.* **1996**, *35*, 840–844.
(44) Kanatzidis, M. G.; Pottgen, R.; Jeitschko, W. *Angew. Chem., Int. Ed.* **2005**, *44*, 6996–7023.
(45) McCarthy, T. J.; Kanatzidis, M. G. *Inorg. Chem.* **1995**, *34*, 1257–1267.

$Yb_5Al_2Sb_6$ indeed are those of a semimetal, and this is supported by the results of DFT electronic structure calculations. This suggests that, despite the convenient description of the compound as a Zintl phase, the electron transfer from the electropositive to the electronegative atoms is incomplete. This is common in this class of compounds, and it is the reason behind the metallic properties encountered in many of them.[46−51] The lattice thermal conductivity of $Yb_5Al_2Sb_6$ is ∼3 W/m K at room temperature, but substitution of only ∼17% of the Yb with Sr cations in the isostructural $Sr_{0.85}Yb_{4.15}Al_2Sb_6$ lowers substantially the thermal conductivity.

Acknowledgment. This project was supported by the U.S. Department of Energy, Office of Science, Basic Energy Sciences under contract no. DE-AC02-06CH11357. A.J.F. thanks the NSF (through its MRSEC program at the N.U. Materials Research Center).

Supporting Information Available: Crystallographic tables and thermal conductivity of $Sr_{0.85}Yb_{4.15}Al_2Sb_6$; additional details of electronic structure calculations. This material is available free of charge via the Internet at http://pubs.acs.org.

(46) Alemany, P.; Llunell, M.; Canadell, E. *J. Comput. Chem.* **2008**, *29*, 2144–2153.
(47) Ge, M. H.; Corbett, J. D. *Inorg. Chem.* **2007**, *46*, 4138–4144.
(48) Li, B.; Corbett, J. D. *J. Cluster Sci.* **2008**, 331–340.
(49) Pan, D. C.; Sun, Z. M.; Mao, J. G. *J. Solid State Chem.* **2006**, *179*, 1016–1021.
(50) Petri, D.; Rohr, C. *Z. Anorg. Allg. Chem.* **2008**, *634*, 1724–1728.
(51) Zelinska, O. Y.; Mar, A. *Inorg. Chem.* **2008**, *47*, 297–305.